Journal of *Marine Science and Engineering*

MDPI

Article

Fine-Scale Geomorphologic Classification of Guyots in Representative Areas of the Western Pacific Ocean

Heshun Wang [1,2], Yongfu Sun [2,*], Shengli Wang [1], Wei Gao [2,*], Weikun Xu [2], Zhen Liu [1], Xuebing Yin [2,3], Sidi Ruan [2,3] and Yihui Shao [2,3]

[1] College of Ocean Science and Engineering, Shandong University of Science and Technology, Qingdao 266590, China; wangheshun@sdust.edu.cn (H.W.); shlwang@sdust.edu.cn (S.W.); liuzhen2016@sdust.edu.cn (Z.L.)
[2] National Deep Sea Center, Qingdao 266237, China; xwk@ndsc.org.cn (W.X.); yinxuebing@hrbeu.edu.cn (X.Y.); s322520026@hrbeu.edu.cn (S.R.); syhlaser@hrbeu.edu.cn (Y.S.)
[3] Qingdao Innovation and Development Base, Harbin Engineering University, Qingdao 266000, China
* Correspondence: sunyongfu@ndsc.org.cn (Y.S.); gaowei@ndsc.org.cn (W.G.)

Abstract: Guyots are a special type of seamount with a flat top and are widely distributed in the global ocean. In this paper, a geomorphologic classification method for guyots based on multibeam bathymetry data is proposed. By studying typical guyots, namely, the Jiaxie Guyots, the Caiwei Guyots, and the DD Guyot in the Western Pacific Ocean, in this study, a multilevel classification system was established, integrating elevation, slope, and bathymetric position index (BPI). The method successfully classified seafloor geomorphology into nine types: summit platform, extremely steep slope, steep slope, gentle slope, very gentle slope, gully on the slope, seafloor plain, local crest, and local depression. Significant differences in the area distribution, depth characteristics, and slope extent of different geomorphologic units in the guyots were revealed by quantitative analysis. The flexibility and accuracy of the method were demonstrated through depth profile validation and method comparison validation. This classification system provides a new cognitive framework for defining the boundaries of seamounts, as well as for the study of the genesis mechanisms of the gullies on the slopes, local crests, and local depressions formed by volcanic activity and other actions.

Keywords: guyots; geomorphologic classification; multibeam bathymetry; Western Pacific Ocean; seamounts

check for updates

Academic Editor: Tom Spencer

Received: 24 March 2025
Revised: 17 April 2025
Accepted: 19 April 2025
Published: 21 April 2025

Citation: Wang, H.; Sun, Y.; Wang, S.; Gao, W.; Xu, W.; Liu, Z.; Yin, X.; Ruan, S.; Shao, Y. Fine-Scale Geomorphologic Classification of Guyots in Representative Areas of the Western Pacific Ocean. *J. Mar. Sci. Eng.* **2025**, *13*, 823. https://doi.org/10.3390/jmse13040823

Copyright: © 2025 by the authors. Licensee MDPI, Basel, Switzerland. This article is an open access article distributed under the terms and conditions of the Creative Commons Attribution (CC BY) license (https://creativecommons.org/licenses/by/4.0/).

1. Introduction

Seamounts are isolated volcanic structures on the seafloor with heights greater than 1000 m and are widely distributed throughout the oceans [1]. It is estimated that there are about 33,452 seamounts worldwide, with more than 400 large seamounts (>3000 m in height, >20 km in diameter, and >3000 km^2 in area), all of which cover up to 20% of the deep seabed [1,2].

Guyots are a specific type of seamount morphology, the concept of which was first introduced by Hess [3]. Guyots have flat tops and are usually interpreted as having been formed by the erosion of seamounts that were once exposed at sea level during subsequent geologic processes [4]. About 60% of Pacific seamounts have flat-topped features, and the slower plate motion in the Western Pacific Ocean makes guyots less susceptible to plate subduction and extinction, which makes the Western Pacific Ocean a typical distribution area for guyots [5–8].

Guyots are initially formed by volcanic activity and gradually sink as a result of cooling action and plate movement [4,9–11]. Guyots generally form in three tectonic settings, namely, near mid-ocean ridges, intraplate volcanisms, and island arcs [9]; most guyots in the Western Pacific Ocean originate from intraplate volcanisms [10,12]. Most magma produced by volcanoes is basaltic magma, and seamount eruptions are predominantly rift eruptions and Hawaiian eruptions [11,13]. The formation of guyots goes through six stages: (1) initial small seamount stage, (2) medium-sized seamount stage, (3) shallow-water eruptive stage, (4) island-forming stage, (5) extinct stage, and (6) subduction stage [4,14,15]. In stage 5, the islands exposed to the sea are gradually submerged due to crustal cooling, subsidence, and erosion, and flat tops may be formed [4]. The cooling and contraction of magma have important implications for the formation of volcanic cones, the accumulation of lava flows, and the distribution of volcanic debris, which have resulted in the formation of gully-riddled geomorphology, distinctly layered terraces, and localized stacked bulges in the seamounts [8,16–18]. In addition, landslides and biochemistry have shaped the rich morphology of guyot surfaces [19,20].

There are numerous guyots in the Western Pacific Ocean, which are rich in inorganic sediments, large biological communities, and microorganisms [21–23]. Seamounts contain large quantities of Eocene Pelagic Limestones and Basaltic Conglomerates, and the tops of guyots are also covered with large quantities of carbonate rocks and foraminiferal oozes, which reflect the process from seamount generation to inundation to deposition [24]. Seamounts are rich in mineral resources such as polymetallic sulfides, manganese nodules, cobalt-rich ferromanganese crusts, and apatite, which are high-grade and polymetallic and are mainly distributed in abyssal plains, slopes, and the tops of seamounts [25,26]. Seamounts with height differences of thousands of meters provide diverse depth space for organisms, and their morphology, which can modify local hydrodynamic conditions, together with the bedrock on the surface of seamounts, is an environmental feature that makes seamount communities richer and more diverse than those in the abyssal plains [27,28]. The spatial heterogeneity of distribution patterns of both mineral and biological resources is closely related to seamount geomorphology, and the accurate identification and classification of seamount geomorphology are the prerequisites for seamount research.

At present, many scholars have carried out work on the classification of guyot geomorphologic types. Masetti et al. [29] presented a methodology for combining bathymetric and backscatter data for seafloor classification. Sowers et al. [30] used the method of Masetti et al. [29] to identify the geomorphology of the Gosnold Guyot, which was categorized into four parts, namely, seamount slope, seamount ridge, seamount valley, and guyot flat. Lundblad et al. [31] proposed the concept of bathymetric position index (BPI), which is a measure of the average elevation of a digital elevation model (DEM) focal unit relative to surrounding units, to identify fine or extensive benthic features using bathymetric position indices at different scales. Fan et al. [32] and Yang et al. [33] used the benthic terrain modeler (BTM) based on Lundblad's theory to classify the fine geomorphologic features of the Caiwei Guyots and the Jiaxie Guyots, respectively, by applying a variety of indexes, including the BPI, to carve the fine geomorphologic features of the guyots.

Existing geomorphologic classification schemes for guyots have certain limitations: some of them are rough; for example, Masetti et al. [29] classified the Gosnold Guyot into only four geomorphologic types. However, as geographic entities with huge morphology, guyots have many detailed features that need to be identified. Some schemes rely on the BTM method and achieve fine-scale classifications, but the accuracy of the classification results is low (Section 5.2). The BTM method identifies the various types in a parameter table on a row-by-row "if. . .else. . ." basis. In addition, these classification schemes lack

generality, and it is difficult to achieve effective comparison and integration, further limiting their application in scientific research and engineering practice.

In this paper, using the deep-sea multibeam data acquired by the multibeam bathymetry system of the China Ocean Mineral Resources R&D Association (COMRA)'s Cruises, a stepwise fine-scale geomorphologic classification method for guyots was established using elevation, slope, and BPI topographic factor indexes, and geomorphologic classifications were carried out for the Jiaxie Guyots, the Caiwei Guyots, and the DD Guyot.

2. Study Areas and Data Acquisition

2.1. Overview of the Study Areas

The topography of the Western Pacific Ocean is complex, and the base diameter of seamounts is generally larger than 20 km; most of them have flat tops, and the height difference of the mountains is more than 2000 m [34].

The Jiaxie Guyots and the Caiwei Guyots are both located in the Magellan Seamount Area. The Magellan Seamount Area is located north of the Mariana Basin in the West Pacific, adjacent to the Mariana Trench to the west, and it consists of nearly 20 seamounts. The seamounts are arranged generally in chains and run NW to SE, with a length of over 1500 km [35]. The Jiaxie Guyots consist of three flat-topped seamounts: Weijia Guyot (also called Ita Mai Tai Guyot), Weixie Guyot (also called Gelendzhik Guyot), and Weizhen Guyot. The largest one is the Weijia Guyot, with a summit platform length and width of about 70 km and 30 km, respectively; the middle-sized one is the Weixie Guyot, with a summit platform length and width of about 30 km and 20 km, respectively; and the smallest one is the Weizhen Guyot, with a summit platform length and width of about 5 km and 2 km, respectively. The depth range of the Jiaxie Guyots is from about 1209 to 6120 m. The Caiwei Guyots consist of two flat-topped seamounts, Caiwei Guyot (also called Pallada Guyot) and Caiqi Guyot. The Caiwei Guyot is the largest, with a summit platform length and width of about 70 km and 35 km, respectively; the Caiqi Guyot is the smallest, with a summit platform diameter of about 15 km. The depth range of the Caiwei Guyots is from about 1230 to 5830 m.

The DD Guyot is located in the vicinity of the Marcus–Wake Seamounts and is a new seamount surveyed during COMRA's Cruise DY86 in 2024. The Marcus–Wake Seamount Area consists of the clustered seamounts along the Marcus Island–Wake Island line in the Western Pacific Ocean [35]. The length and width of the summit platform of the DD Guyot are about 10 km and 7 km, respectively, and the depths range from 1037 to 6289 m.

The detailed locations of the Jiaxie Guyots, the Caiwei Guyots, and the DD Guyot are shown in Figure 1.

2.2. Data Acquisition

The data used in this paper come from deep-sea multibeam surveys of the seamounts of the Western Pacific Ocean during COMRA's Cruises DY31, DY35, DY66, DY80, and DY86. The multibeam equipment used is the EM124 full-depth multibeam sounder from Kongsberg, which operates at 12 kHz, has a bathymetric range of 20 to 11,000 m, has a maximum swath width of 6 times the water depth, has a bathymetric accuracy of 0.6% of the water depth, and has excellent performance in full-depth seafloor topographic mapping. The multibeam data were processed using CARIS HIPS and SIPS 11.4 (https://www.teledynecaris.com/, accessed on 1 July 2024), and the resolution of the DEM data for the Jiaxie Guyots, the Caiwei Guyots, and the DD Guyot was ~50 m, ~200 m, and ~50 m.

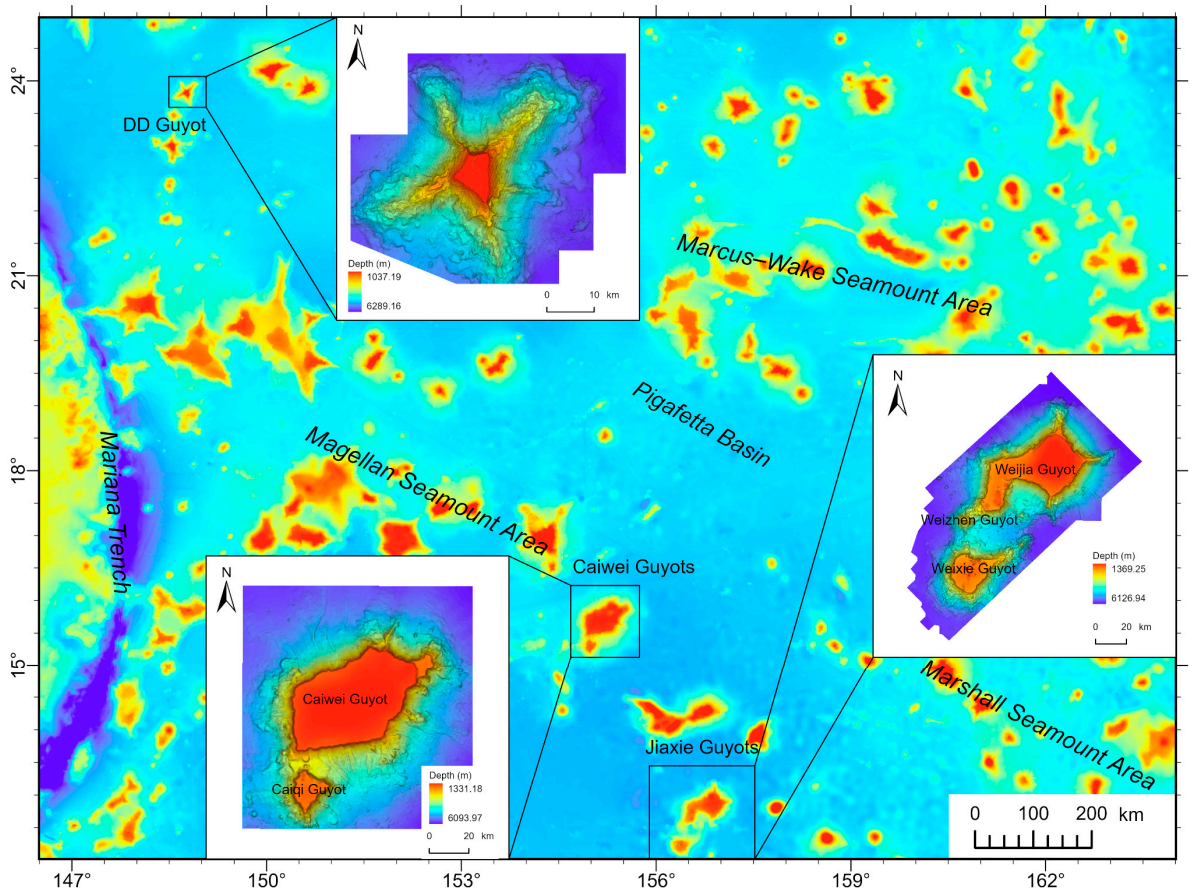


Figure 1. Locations of the Jiaxie Guyots, the Caiwei Guyots, and the DD Guyot. Depth data were obtained from COMRA's Cruises.

3. Geomorphologic Classification Methods

3.1. Design of Geomorphologic Classification

The geomorphologic structure of guyots is complex and diverse, and the distribution of guyot mineral and biological resources is closely related to the elevation, slope, gully, ridge, and other areas. Given this, in this paper, the geomorphology of seamounts is defined as the types shown in Table 1 concerning several recommendations and specifications on geomorphology classification, including, but not limited to, *The second world ocean assessment* (United Nations) [36,37], *Rules for classification and coding of geomorphological types* (China) [38], and the research of scholars such as Sowers et al. [30]. Because ridges contain multiple patterns of topographic relief and change, and because the exact boundaries of ridges are not easy to determine, in this paper, ridgelines are used on the geomorphologic classification maps to identify the length and orientation of ridges.

According to the definition in Table 1, the three topographic factors of elevation, slope, and BPI were selected to be used for the geomorphologic classification of guyots. The general classification idea was as follows (Figure 2): The DEM data of the guyots were input to extract the topographic factors. Subsequently, the preliminary geomorphologic classification based on elevation and slope yielded six geomorphologic regions, such as the summit platform, and the fine geomorphologic classification based on elevation, slope, and BPI yielded three geomorphologic types, such as local crest. Finally, these nine geomorphological types were plotted on the map, analyzed, and discussed. The relevant subsection headings are labeled in Figure 2.

Table 1. Geomorphologic types of guyots.

Large-Scale	Fine-Scale	Description	Slope Range (°)	stdBPI Range
Summit	Summit platform	Areas of flat or nearly flat terrain on top of seamounts are usually characterized by a broad plateau or flat top with a slope of less than 5°.	0~5	−100~100
Flank	Extremely steep slope	Areas with slopes greater than 25°.	>25	−100~100
	Steep slope	Areas with slopes greater than 15° and less than 25°.	15~25	−100~100
	Gentle slope	Areas with slopes greater than 5° and less than 15°.	5~15	−100~100
	Very gentle slope	Areas with slopes less than 5°.	0~5	−100~100
	Ridge	Narrow and elevated lines of terrain.		>100
	Gully on the slope	Narrow lowlands formed by erosion or tectonic cutting.		<−100
Bottom	Seafloor plain	Areas of flat topography at the base of seamounts, with slopes generally less than 2°.	0~2 [1]	−100~100
	Local crest	Raised terrains with a high center and a low periphery formed by tectonics or accretion.		>100
	Local depression	Depressed terrains with a low center and a high surrounding area formed by tectonics or erosion.		<−100

[1] Seafloor plains will contain a small number of areas with slopes greater than 2°.

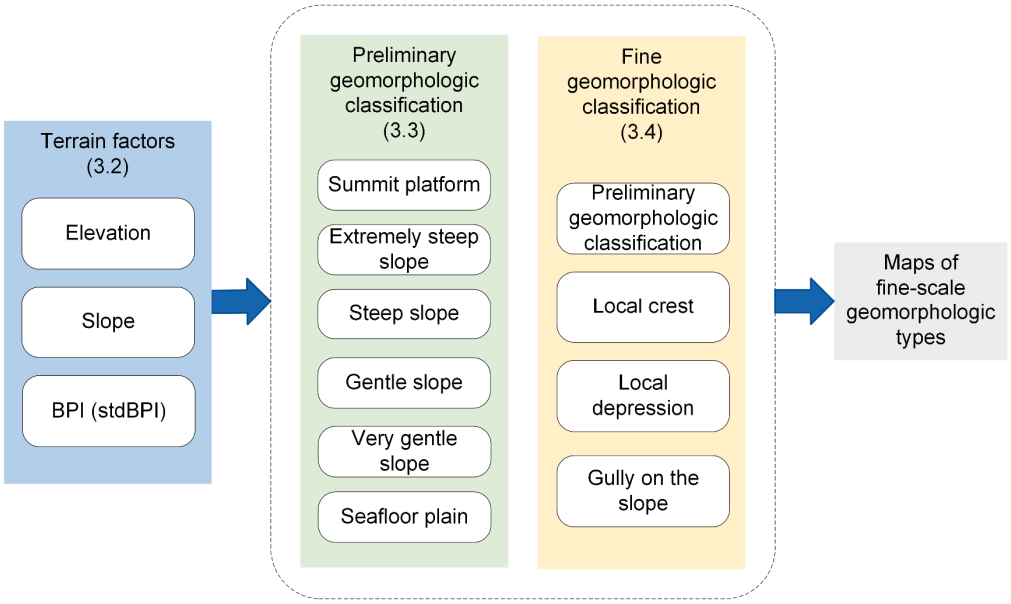


Figure 2. Methodological framework for the geomorphologic classification of guyots in representative areas of the Western Pacific Ocean.

3.2. Calculation of Terrain Factors

3.2.1. Elevation

Elevation is the distance from a point on the ground surface along the plumb line to the geodetic level. It is one of the most basic topographic factors of geomorphologic patterns, and its size directly reflects the high and low undulation of geomorphologic entities [39]. The elevation data were obtained directly from the DEM.

3.2.2. Slope

Slope is the degree of inclination of a localized surface slope. It is one of the basic characteristics of a surface geomorphologic entity [40] and is usually expressed as an inverse trigonometric function of the ratio of the vertical elevation difference and the horizontal distance. The expression of slope is

$$Slope = \arctan\sqrt{\left(\frac{\partial z}{\partial x}\right)^2 + \left(\frac{\partial z}{\partial y}\right)^2} \quad (1)$$

where $\frac{\partial z}{\partial x}$ and $\frac{\partial z}{\partial y}$ are the first-order derivatives of the elevation with respect to the x and y directions.

3.2.3. BPI

The BPI is an index used to characterize seafloor topography by comparing the elevation of a location with the average elevation of its surrounding area to determine whether the location is above, below, or similar to the surrounding topography [31]. The BPI was modified from the topographic position index as defined by Weiss [41] and Iampietro and Kvitek [42]. It is widely used in seabed geology, biology, ecology, and environmental research [43–45]. The expression for the calculation of the BPI is

$$BPI = \text{int}(bathy - \text{focalmean}(bathy, r_i, r_o) + 0.5) \quad (2)$$

where int denotes downward rounding, $bathy$ is the depth value of a grid cell, focalmean is used to calculate the depth value of the annulus around the grid cell, r_i is the inner radius of the BPI calculation (the length is the number of pixels, which can be zero), r_o is the outer radius of the BPI calculation, and 0.5 is a rounding adjustment term.

According to the BPI theory [31,46], the BPI has to be normalized to obtain the standardized BPI (stdBPI) when it is used in practice, which is a major feature of BPI in practice. The expression for the calculation of the stdBPI is

$$stdBPI = \text{int}\left(\left(\frac{BPI - \overline{X}_{BPI}}{\sigma_{BPI}}\right) \cdot 100 + 0.5\right) \quad (3)$$

where int denotes downward rounding, $\overline{X}_{BPI}$ is the average of all grid cell BPIs, σ_{BPI} is the standard deviation of all grid cell BPIs, 100 is a scaling factor used to convert standardized BPIs to a more interpretable scale, and 0.5 is a rounding adjustment term.

By standardization, it can be classified with uniform thresholds. Specifically, the local crest needs to satisfy the condition that the stdBPI is greater than 100, and the local depression and gully on the slope need to satisfy the condition that the stdBPI is less than -100.

When calculating the BPI (stdBPI), how to select the size of the inner and outer radii is not yet conclusive and is now generally determined by the trial-and-error method [32]. Mena et al. [47] suggested that the radius of the BPI calculation be set to approximate the size of the target morphology and concluded that different shapes of the analyzed neighborhoods (ring and circle) have no significant effect on the results. Based on the above theory, as well as the experience of others in using the BPI, the diameters of medium-sized crests and depressions were selected as the outer radius ratio factor of BPI calculation (Radius Ratio Factor of BPI Calculation = Radius of BPI calculation × DEM Data Resolution), and in order to simplify the calculations, the inner radius of the calculation of the BPI was set to 0. The specific setup scheme is shown in Table 2.

Table 2. Outer radius of BPI calculation for different guyots.

Guyot	Outer Radius of BPI Calculation
Jiaxie Guyots	30
Caiwei Guyots	10
DD Guyot	12

Figure 3 illustrates the elevation, slope, and stdBPI of the Jiaixe Guyots, the Caiwei Guyots, and the DD Guyot.

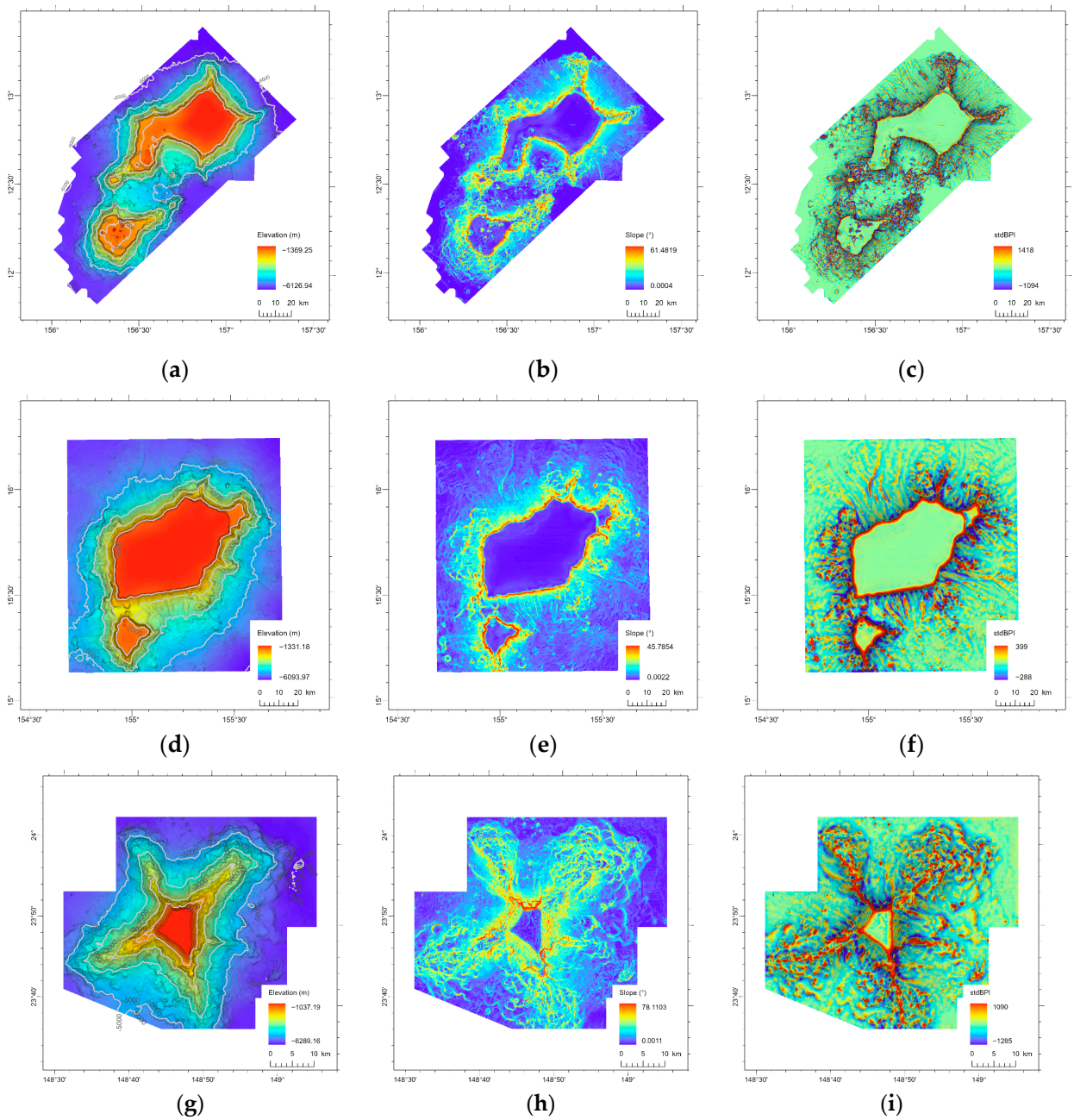


Figure 3. Terrain factors of the Jiaxie Guyots, the Caiwei Guyots, and the DD Guyot: (**a**) Elevation of the Jiaxie Guyots; (**b**) Slope of the Jiaxie Guyots; (**c**) stdBPI of the Jiaxie Guyots; (**d**) Elevation of the Caiwei Guyots; (**e**) Slope of the Caiwei Guyots; (**f**) stdBPI of the Caiwei Guyots; (**g**) Elevation of the DD Guyot; (**h**) Slope of the DD Guyot; (**i**) stdBPI of the DD Guyot.

3.3. Preliminary Geomorphologic Classification Based on Elevation and Slope

According to the definition in Table 1, the areas with slopes of 0~2° in the DEM data are extracted to form the initial candidate area. Using the image recognition algorithm, the regions close to the edge of the data were extracted, and the slope threshold condition was satisfied in the initial candidate region to construct the initial seafloor plain mask. Aiming at the local slope anomalies existing in the initial mask (e.g., a small range of areas with a slope greater than 2°), the area filling technology was used to incorporate the anomalies that were surrounded by the seafloor plains into the range of the seafloor plains. Through processing, the problem of recognizing the fuzzy boundary of the submarine plain–seamount transition zone was effectively solved. The process is shown in Figure 4.

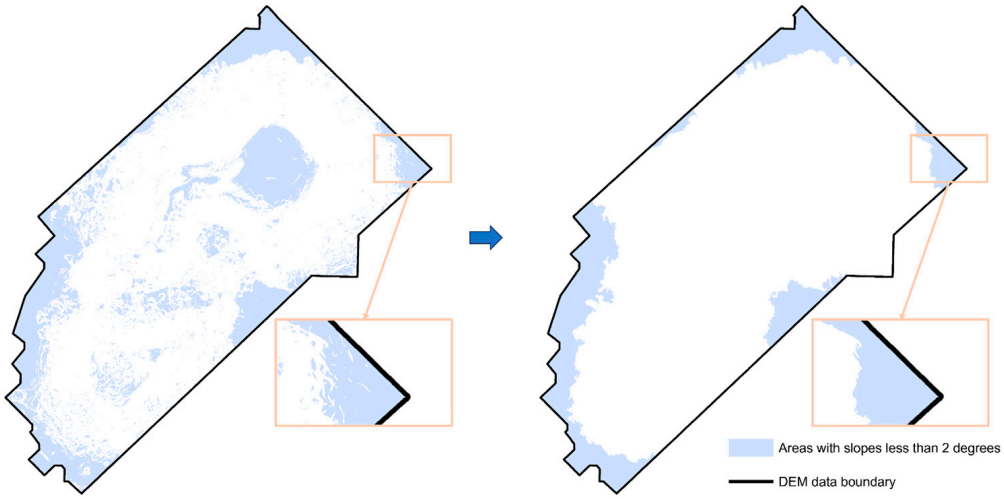


Figure 4. Extraction of seafloor plains. Areas with slopes less than 2 degrees that were not near the DEM data boundary were excluded, and small blank areas surrounded by areas with slopes less than 2 degrees were still identified as seafloor plains.

Patchy areas with slopes of 0~5° were extracted from the DEM data, and these areas were arranged according to the elevation mean value from the largest to the smallest, and examined one by one to see whether they were summit platform areas until a complete summit platform was found. The process is shown in Figure 5.

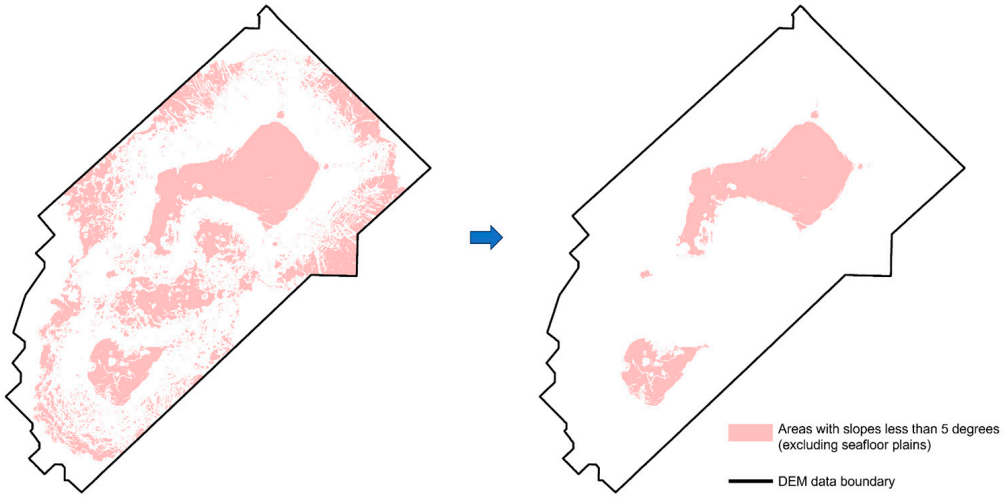


Figure 5. Extraction of summit platforms. Areas with slopes less than 5 degrees were sorted by elevation from highest to lowest to obtain the summit platform area.

After identifying seafloor plains and summit platforms, the other parts were noted as regional flanks, and the slope was classified. Flank can be divided according to the slope thresholds in Table 1. Even though the summit platform, very gentle slope, and seafloor plain contain the same slope values, the three are not confused with each other because of their slopes through a stepwise process.

Through the process described in this subsection, guyots were successfully classified as summit platform, extremely steep slope, steep slope, gentle slope, very gentle slope, and seafloor plain.

3.4. Fine Geomorphologic Classification Based on Elevation, Slope, and BPI

Guyots are distributed with obvious crested and depressed areas, which can be recognized by using stdBPI. Figure 6 shows a schematic longitudinal section of the seamount area, and the letters A to H denote local crests, feet of guyots, summit edges, summit platforms, uniform slopes, local depressions, seafloor plains, and the edge areas of DEM data, respectively. According to the BPI theory [31], the recognition results of these eight zones are shown in Table 3.

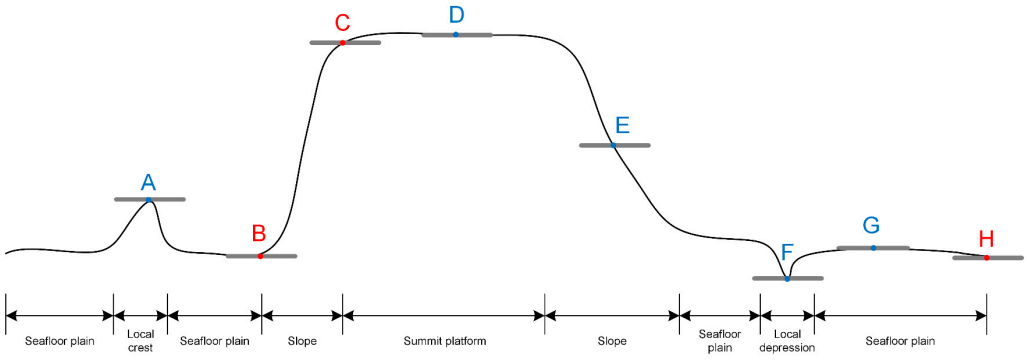


Figure 6. Schematic of the longitudinal section of guyots (according to Lundblad et al. [31]). The horizontal gray line segment indicates the diameter of the BPI calculation. The stdBPI values and identification results for each point are displayed in Table 3.

Table 3. Longitudinal section identification results of Figure 4.

Point	stdBPI Value	Identification Result	Comparison with the Actual Situation
A	>100	Crest	Consistent
B	<−100	Depression	Inconsistent
C	>100	Crest	Inconsistent
D	−100~100	Constant slope zone	Consistent
E	−100~100	Constant slope zone	Consistent
F	<−100	Depression	Consistent
G	−100~100	Constant slope zone	Consistent
H	<−100	Depression	Inconsistent

From Figure 6 and Table 3, it can be seen that stdBPI has no problem recognizing the geomorphology results for points A, D, E, F, and G of the guyots. However, for points B, C, and H, i.e., the feet of guyots, summit edges, and data edges, the classification results are inaccurate. Point B has a seafloor plain to the left and a slope to the right, which leads to an stdBPI of less than −100 for point B and its immediate vicinity. Point C has a slope to the left and a summit platform to the right, which leads to an stdBPI of more than 100 for point C and its immediate vicinity. Point H has a slightly sloped seafloor plain to the left, with no depth data on the right, which leads to an stdBPI of less than −100. Therefore, if the geomorphologic types are classified only according to the stdBPI threshold, erroneous

results will be obtained in some areas. There are also gullies on the slopes, which are often thought to be transportation routes for sediments [48], and the type needs to be identified.

In this paper, a processing method is proposed that extracts the crests and depressions recognized by the stdBPI and identifies gullies on the slopes, local crests, and local depressions. For the identification of local crests (or local depressions), the steps are as follows:

1. Extract elevation data for a range of 200 × 200 m from the center of each crest (or depression), then calculate the average value.
2. Extract the elevation value of the crest (or depression) at the edge.
3. Compare the data values. If the average value of the elevation in the 200 × 200 m range in the center area is greater (or smaller) than the maximum value (or minimum value) in the edge area, the area is judged to be a local crest (or local depression).

For the identification of gullies on the slopes, the steps are as follows:

1. Extract the elevation values of each point on the centerline of each depression and calculate its average value, denoted as AVE1.
2. Extract the elevation value of the depression at the edge and calculate its average value, denoted as AVE2.
3. Compute the slope of the line connecting the highest point of the elevation and the lowest point of the elevation on the centerline, denoted as SLO.
4. Compare the data values. If AVE1 is smaller than AVE2 and SLO is greater than 10° [8], the area is determined to be a gully on the slope.

Figure 7 illustrates the identification of local crests, local depressions, and gullies on the slopes. The red area is a 200 × 200 m area in the center of the crest, and its elevation average is compared with the elevation value of the edge surrounded by the green circle, and those areas that meet the conditions are identified as localized bumps. The blue area is also the area of 200 × 200 m in the center of the depression, and the average value of its elevation is compared with the elevation value of the edge surrounded by the green circle. An area is recognized as a local depression if it meets the conditions. The yellow line is the middle line of the depression, and its value is compared with the value of the outermost circle of the green area; those areas that meet the conditions are recognized as gully areas.

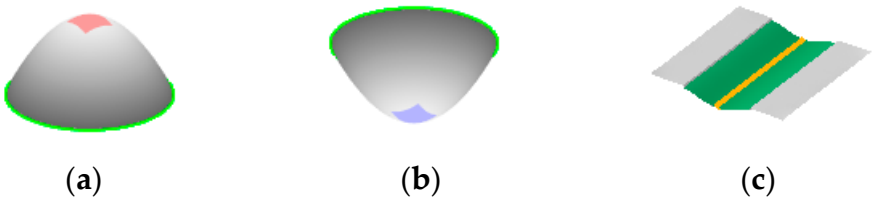


Figure 7. The diagrams of (**a**) local crest, (**b**) local depression, and (**c**) gully on the slope. The elevation values of the red area of 200 × 200 m at the center of (**a**) are compared with the green edge area. The elevation values of the blue area of 200 × 200 m at the center of (**b**) are compared with the green edge area. The SLO and mean elevation values for the yellow centerline of (**c**) need to be met.

The above steps are realized after the stdBPI is roughly judged. If there is no antecedent BPI foundation, it is difficult to achieve the ideal effect. After the comparison and screening of the stdBPI, the elevation, slope, local crests, local depressions, and gullies on the slopes in the guyots can be accurately identified.

Through the above stepwise geomorphologic classification, the problem of a lack of flexibility while obtaining fine-scale geomorphologic classification results is avoided. At the same time, the thresholds used in each classification step of this paper are standardized indicators, which have good generality for most guyots.

4. Results

In this study, preliminary geomorphologic classification results and fine geomorphologic classification results were obtained (Figures 8–10 and Tables 4–6). The preliminary geomorphologic classification results classified the seamounts into six major areas: summit platform, extremely steep slope, steep slope, gentle slope, very gentle slope, and seafloor plain. The fine geomorphologic classification results show the geomorphologic information of the local crest, local depression, and gully on the slope. Ridgelines are labeled on the fine geomorphologic classification results, and there are significant length differences in the ridgelines of different guyots. The width of the gullies on the slopes in the guyots in the study area of this paper is generally 500~1000 m, and the diameters of local crests and local depressions are generally within 2 km. Three-dimensional maps of the geomorphologic types for guyots are provided in Appendix A (Figures A1–A3).

4.1. Jiaxie Guyots

In the classification results, gentle slopes have the largest area of 4155.56 km^2 (33.23%) and local depressions have the smallest area of 4.00 km^2 (0.03%). Gullies on the slopes are mainly concentrated between extremely steep slopes and steep slopes, and the distribution of elevation is relatively uniform; local crests and local depressions have the largest standard deviation of elevation, and it can be seen that they are distributed from the top to the bottom of the guyot body. The slope distributions in these areas of summit platforms, steep slopes, gentle slopes, and very gentle slopes are more uniform, while the slope distributions in these areas of extremely steep slopes, gullies on the slopes, seafloor plains, local crests, and local depressions are closer to their own slope minimum. The Jiaxie Guyots have four distinctly developed ridges, three of which belong to the Weijia Guyot and one to the Weixie Guyot.

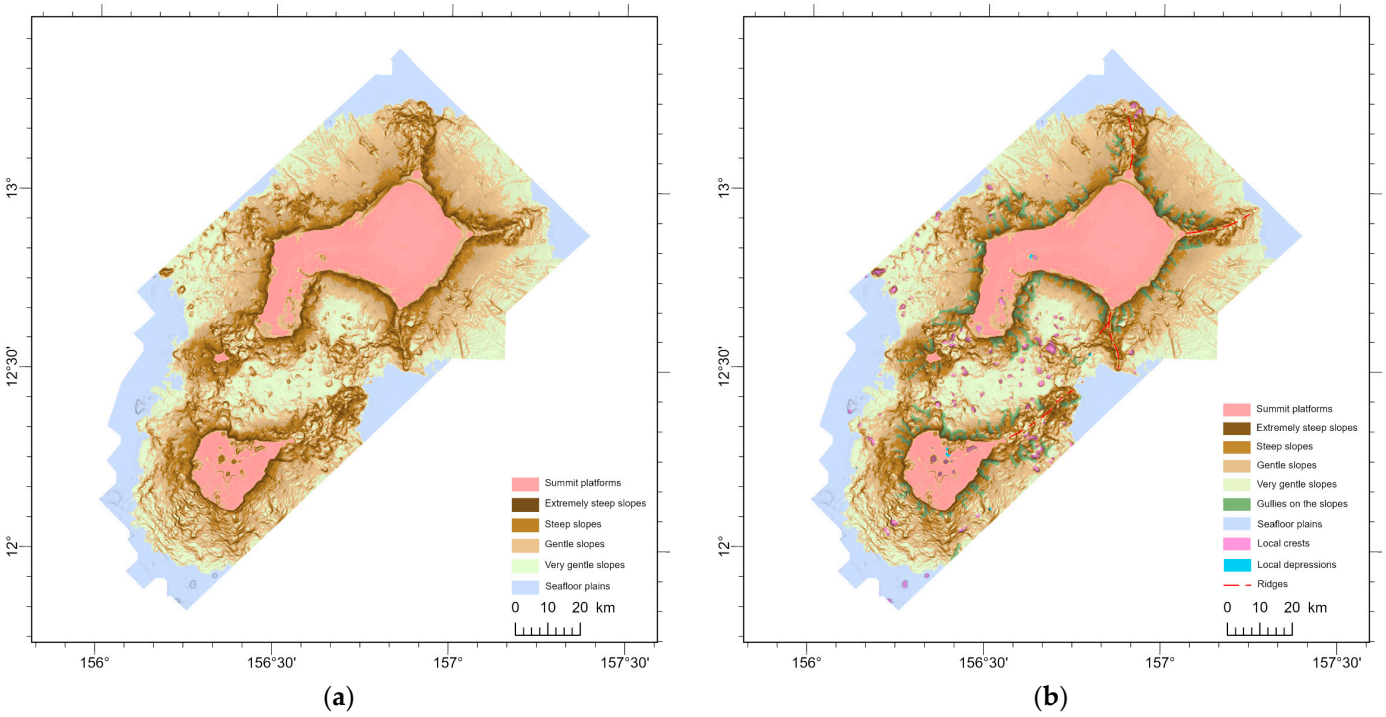


Figure 8. Results of the geomorphologic classification of the Jiaxie Guyots: (**a**) Preliminary, (**b**) Fine.

Table 4. Statistics of the geomorphologic classification of the Jiaxie Guyots.

Geomorphologic Type	Area (km^2)	Area (%)	Depth		Slope		
			Mean (m)	Std	Min (°)	Max (°)	Mean (°)
Summit platform	1591.89	12.73	1746.98	253.48	0.00	5.00	2.08
Extremely steep slope	619.87	4.96	3333.74	1017.48	25.00	61.48	29.20
Steep slope	1886.68	15.09	3848.62	979.45	15.00	25.00	19.36
Gentle slope	4155.56	33.23	4558.11	1032.53	5.00	15.00	9.34
Very gentle slope	2367.07	18.93	5336.53	620.87	0.00	5.00	2.97
Gully on the slope	526.56	4.21	3635.93	818.01	0.03	54.54	17.87
Seafloor plain	1885.54	15.08	5978.82	82.83	0.00	23.68	0.82
Local crest	134.52	1.08	4303.62	1251.96	0.07	42.55	14.98
Local depression	4.00	0.03	3053.34	1628.86	0.05	32.32	6.32

Total area = summit platform area + extremely steep slope area + steep slope area + gentle slope area + very gentle slope area + seafloor plain area.

4.2. Caiwei Guyots

The very gentle slopes of the Caiwei Guyots have the largest area of 4594.66 km^2 (34.34%), while the smallest area of 6.72 km^2 (0.05%) still belongs to local depressions. The summit platforms are extremely flat, with a standard deviation of elevation of only 126.86 and a mean slope of only 0.95°. The distribution pattern of slopes and depths is consistent with that of the Jiaxie Guyots. Localized bumps and localized depressions are mainly distributed in the areas of gentle slopes and below. The ridge feature of the Caiwei Guyots is not obvious enough, and seven small ridges have been identified.

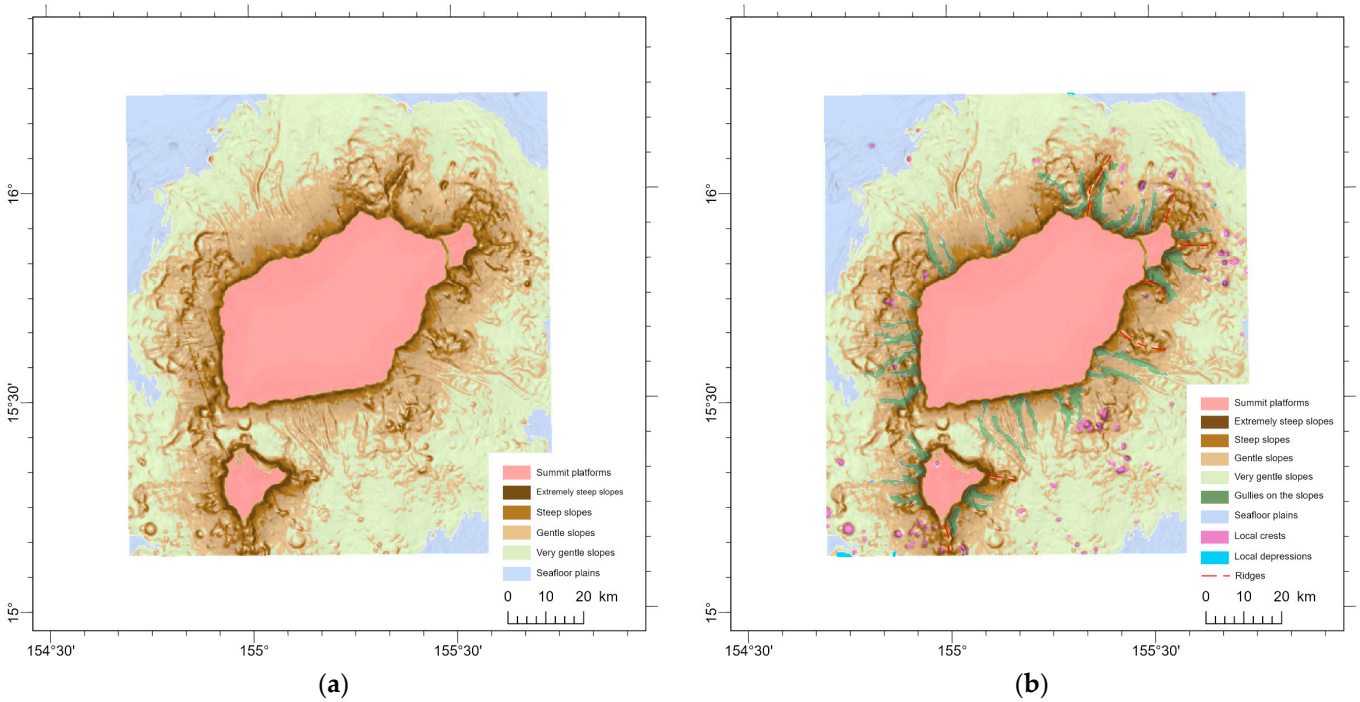


Figure 9. Results of the geomorphologic classification of the Caiwei Guyots: (**a**) Preliminary, (**b**) Fine.

Table 5. Statistics of the geomorphologic classification of the Caiwei Guyots.

Geomorphologic Type	Area (km^2)	Area (%)	Depth		Slope		
			Mean (m)	Std	Min (°)	Max (°)	Mean (°)
Summit platform	2167.64	16.20	1435.86	126.86	0.00	5.00	0.95
Extremely steep slope	269.85	2.02	2407.10	679.92	25.00	45.79	28.48
Steep slope	1146.34	8.57	3101.05	853.36	15.00	25.00	19.01
Gentle slope	3851.27	28.79	4126.17	870.33	5.00	15.00	9.02
Very gentle slope	4594.66	34.34	5128.10	513.00	0.02	5.00	2.88
Gully on the slope	527.86	3.95	3311.81	682.79	1.62	42.48	13.75
Seafloor plain	1348.81	10.08	5704.51	193.14	0.00	13.37	1.27
Local crest	138.16	1.03	4713.02	726.81	0.14	30.67	10.87
Local depression	6.72	0.05	5331.84	257.20	0.22	7.87	3.93

Total area = summit platform area + extremely steep slope area + steep slope area + gentle slope area + very gentle slope area + seafloor plain area.

4.3. DD Guyot

The largest part of the DD Guyot is characterized by gentle slopes, with an area of 823.18 km^2 (35.85%); the smallest part still belongs to localized depressions, with an area of 1.22 km^2 (0.05%). The summit platforms of the DD Guyot have a relatively small area of 28.49 km^2 (1.24%). The DD Guyot has a large number of extremely steep slopes and is overall steeper. Local crests are generally distributed on gentle slopes and in the area below. The elevation standard deviation of the local depressions is large, and it is seen to be distributed in several elevation regions of the guyot. The DD Guyot develops five distinct ridges that spread out in all directions.

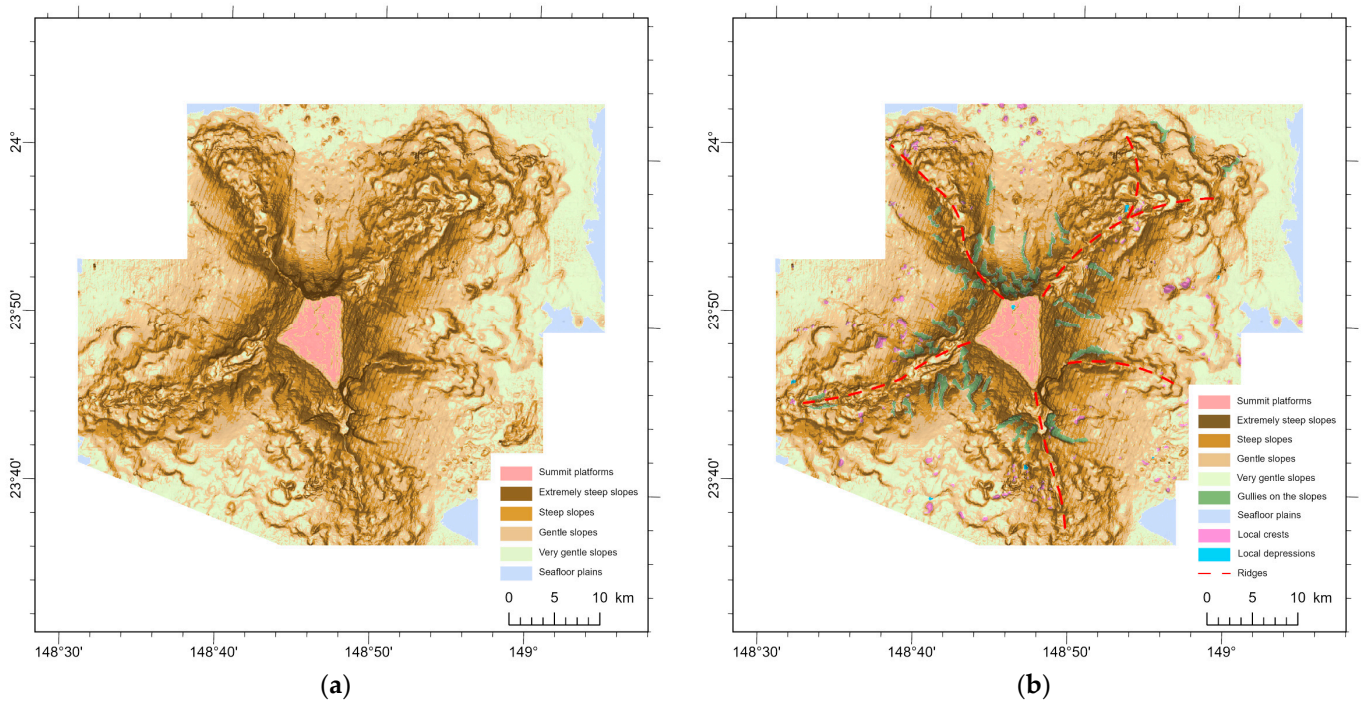


Figure 10. Results of the geomorphologic classification of the DD Guyot: (**a**) Preliminary, (**b**) Fine.

Table 6. Statistics of the geomorphologic classification of the DD Guyot.

Geomorphologic Types	Area (km^2)	Area (%)	Depth		Slope		
			Mean (m)	Std	Min (°)	Max (°)	Mean (°)
Summit platform	28.49	1.24	1081.10	16.06	0.00	5.00	2.38
Extremely steep slope	367.22	15.99	3485.88	1102.69	25.00	78.11	31.48
Steep slope	519.98	22.65	4130.57	981.30	15.00	25.00	19.68
Gentle slope	823.18	35.85	4808.42	904.72	5.00	15.00	9.64
Very gentle slope	501.48	21.84	5492.92	548.79	0.00	5.00	2.83
Gully on the slope	54.68	2.38	3425.28	789.23	0.94	75.79	26.04
Seafloor plain	55.51	2.42	5872.68	51.65	0.00	32.03	1.44
Local crest	20.32	0.89	4822.67	815.18	0.31	64.90	17.38
Local depression	1.22	0.05	4140.55	1519.86	0.13	39.33	12.41

Total area = summit platform area + extremely steep slope area + steep slope area + gentle slope area + very gentle slope area + seafloor plain area.

5. Discussion

5.1. Validation of Geomorphologic Classification Results

To verify the accuracy of the classification results, the depth profiles at the Jiaxie Guyots, the Caiwei Guyots, and the DD Guyot (Figures 11 and 12 and Lines AB, CDEF, and GH) are plotted, and the profiles are labeled with a system of alphabetic symbols at key geographic nodes (a~j).

In Figures 11 and 12, "a" is the edge of the summit without the classification error shown in Figure 6; the geomorphologic type of zones "b" and "c" is local crest; the geomorphologic type of zone "d" is local depression; zones "e"~"g" are gullies on the slopes; and zones "h"~"j" indicate the stepped geomorphologic features of the DD Guyot. By observing and comparing the depth profile characteristics in Figures 11 and 12, it can be seen that the method proposed in this paper shows good applicability in all three guyot areas, which reflects the reliability of this method.

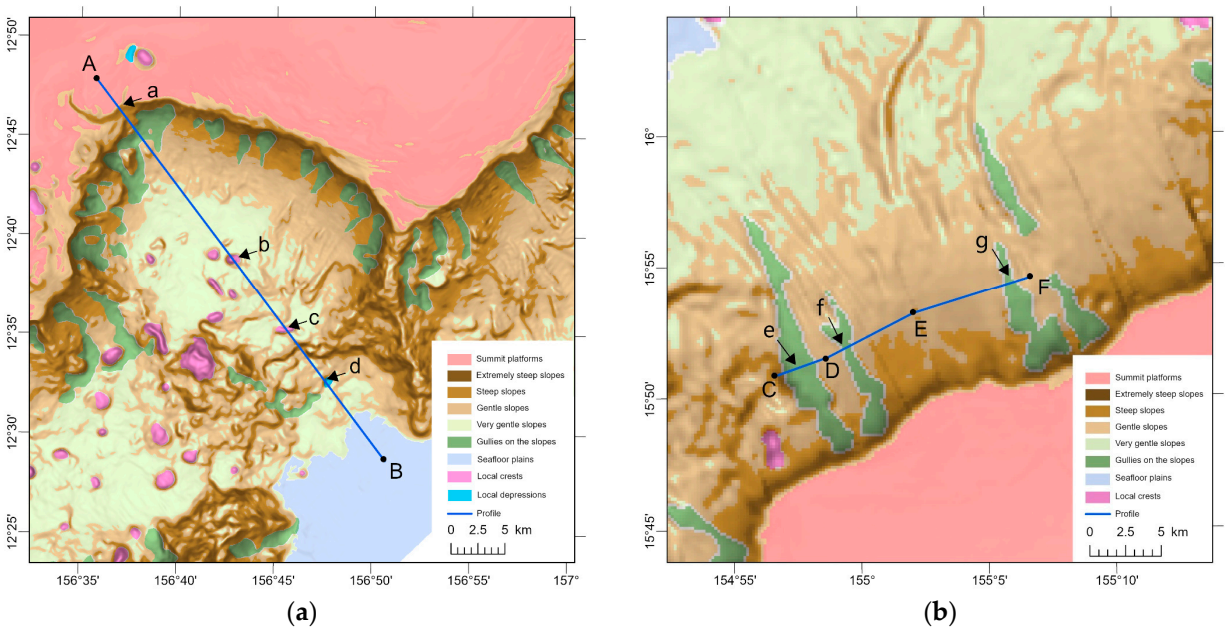
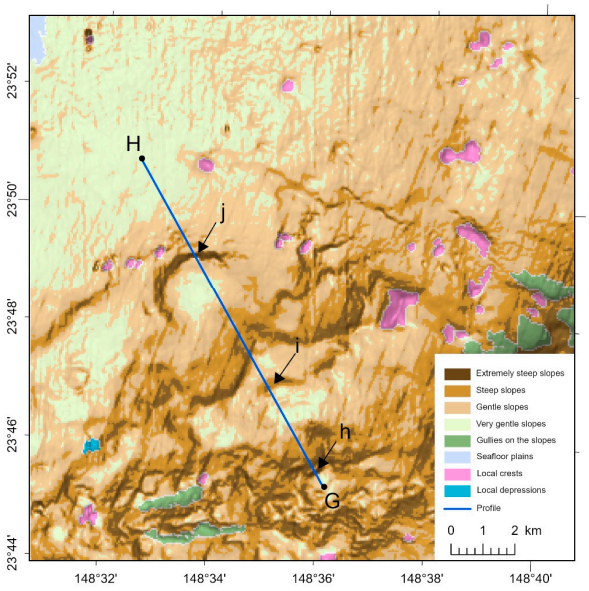
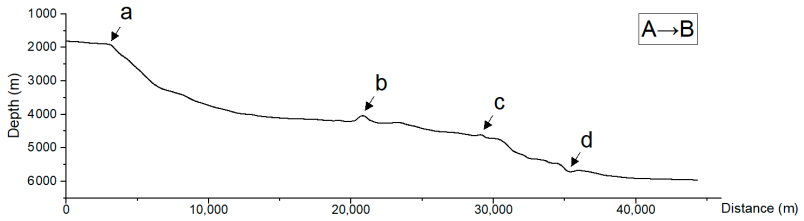


Figure 11. *Cont.*

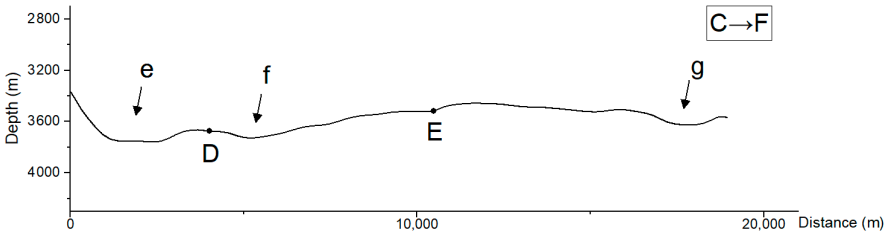


(**c**)

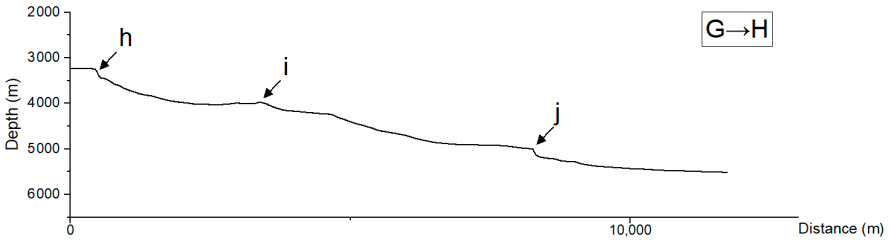
Figure 11. Location of guyot depth profiles: (**a**) the Jiaxie Guyots, (**b**) the Caiwei Guyots, and (**c**) the DD Guyot.



(**a**)



(**b**)



(**c**)

Figure 12. Guyot depth profiles of Figure 11: (**a**) Line AB, (**b**) Line CDEF, and (**c**) Line GH. The letters in the figure need no additional explanation.

5.2. Comparison with the BTM Method

To verify the effectiveness of this paper's method in geomorphology classification, in this paper, BTM for geomorphology classification is used for comparison. The parameters

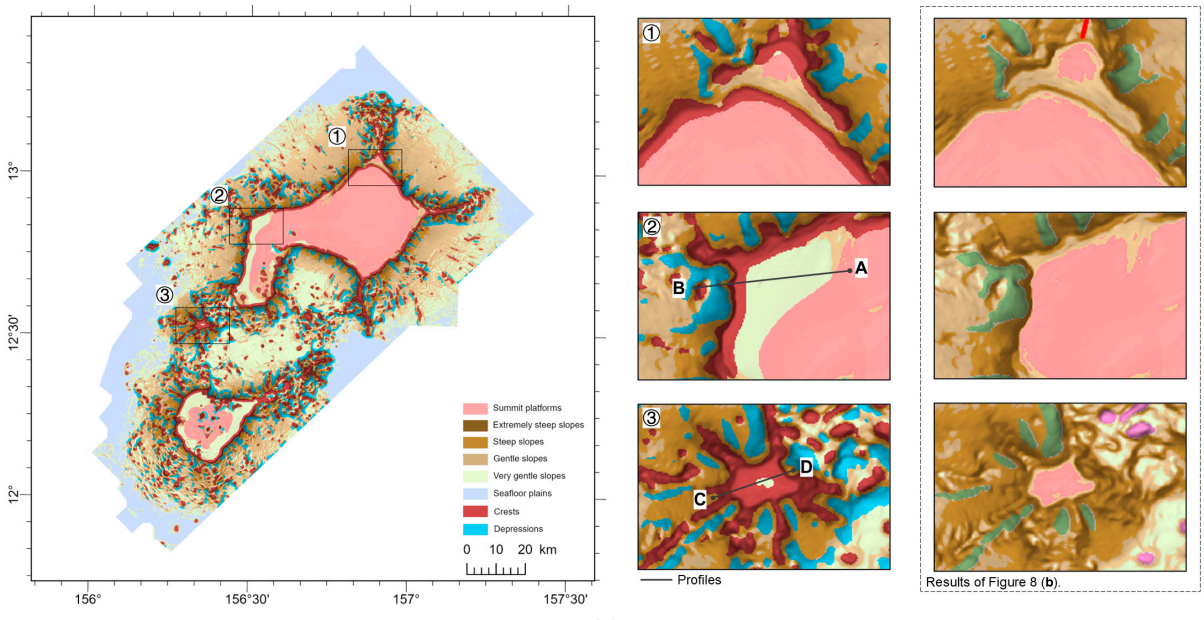
are set in Table 7 [32,33], and the classification results are shown in Figure 13. The settings of the outer radius of the BPI calculation are the same as in Table 2. The fine geomorphologic classification of Section 3.4 could not be achieved using the BTM method. Therefore, the gully on the slope, local crest, and local depression geomorphology types were dropped, and the crest and depression geomorphology types were newly set. The comparison results are presented in Figure 13.

Table 7. Parameters of terrain factors for the BTM method.

Geomorphologic Type	BPI		Slope (°)		Elevation (m)	
	Lower	Upper	Lower	Upper	Lower	Upper
Summit platform	−100	100	0	5	−2000	
Seafloor plain	−100	100	0	2		−5500
Extremely steep slope	−100	100	25			
Steep slope	−100	100	15	25		
Gentle slope	−100	100	5	15		
Very gentle slope	−100	100	0	5		
Crest	100					
Depression		−100				

In Figure 13, it can be seen that the edge areas of summit platforms are recognized by the BTM as crests, which obscures the area of extremely steep slopes (1, 2, 3, and 5); the ranges of summit platforms and seafloor plains are inaccurate due to elevation thresholds set on the high side or the low side (2 and 3); the seafloor plains and the very gentle slopes at the base of the mountain appear to contain each other (4 and 7); areas of stepped landforms tend to be recognized as alternating crests and depressions (5 and 8); and slopes located at the edge of the data are recognized as depressions (6). The problems shown in Figure 13 are solved by the treatment in Section 3 of this paper.

Figure 14 plots the depth profiles identified in Figure 13. The profiles clearly demonstrate the shortcomings of the BTM method and the advantages of the method proposed in this paper.



(**a**)

Figure 13. *Cont.*

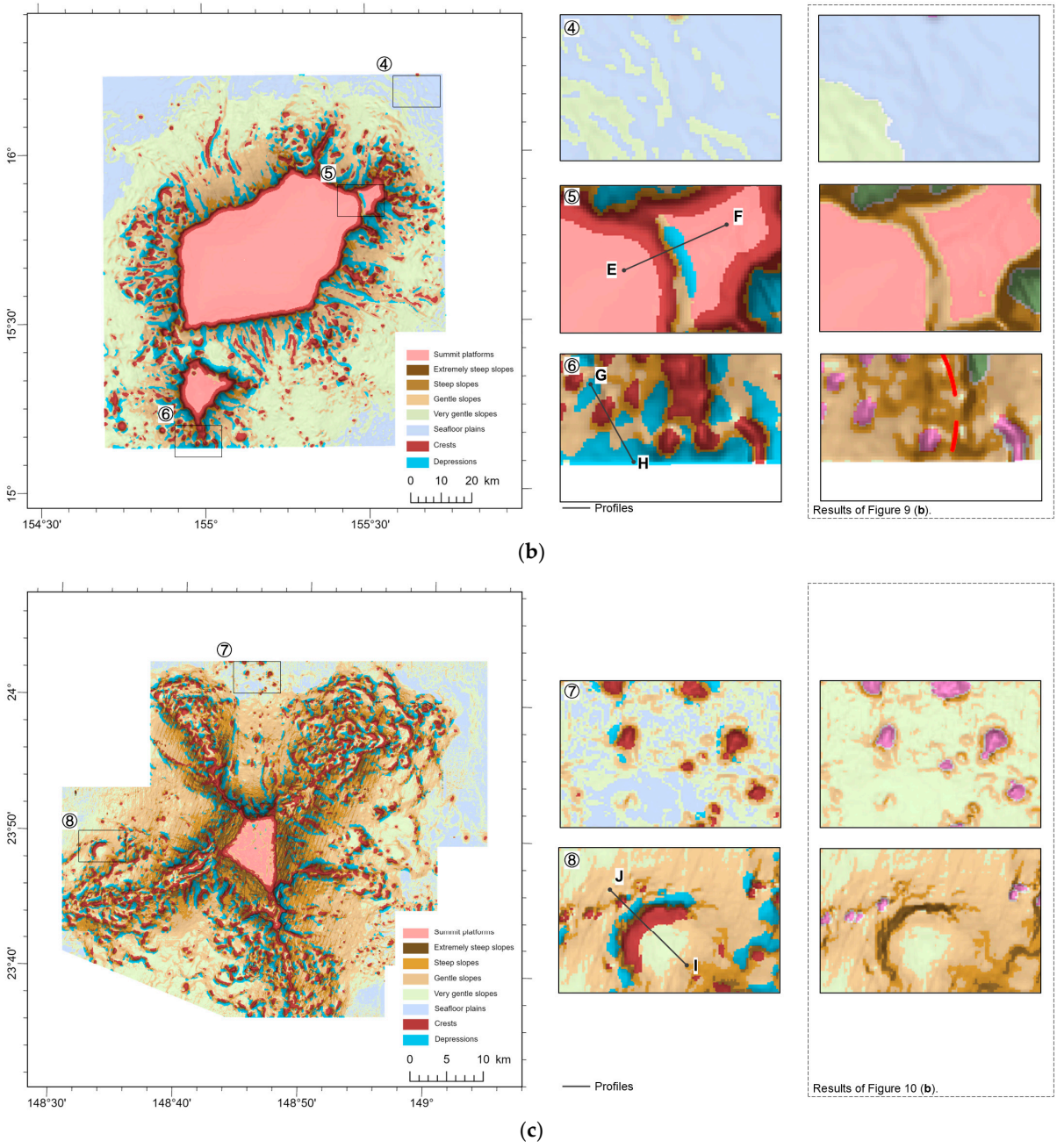


Figure 13. Results of geomorphologic classification using the BTM method (with comparison): (**a**) the Jiaxie Guyots, (**b**) the Caiwei Guyots, and (**c**) the DD Guoyt. Refer to Figures 8–10 for illustrations of the images in the rightmost dashed box.

5.3. Overall Geomorphological Features of Guyots

The Jiaxie Guyots and the Caiwei Guyots contain larger summit platforms with more gentle overall slopes. However, it can be seen that the DD Guyot is the steepest guyot and is significantly larger than the Jiaxie Guyots and the Caiwei Guyots in terms of both the difference in elevation and the average gradient (Figure 15). This may be closely related to the process of guyot formation. According to the theory of guyot formation [4,14,15], volcanoes that are less exposed to the sea are subjected to less erosion, ultimately retaining steeper and extremely steep slopes. This may also be related to the state of the volcano at the time of eruption [9–12].

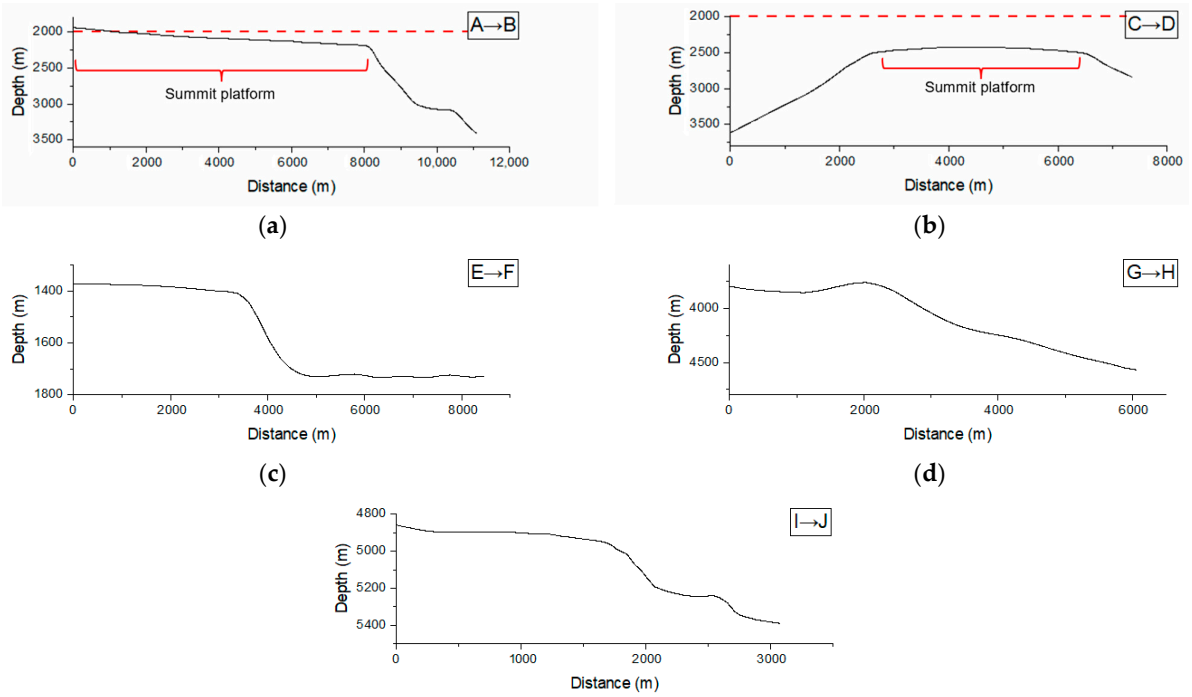


Figure 14. Guyot depth profiles of Figure 13: (**a**) Line AB, (**b**) Line Cd, (**c**) Line EF, (**d**) Line GH, and (**e**) Line IJ. The red dashed line represents the −2000 m elevation threshold from Table 7.

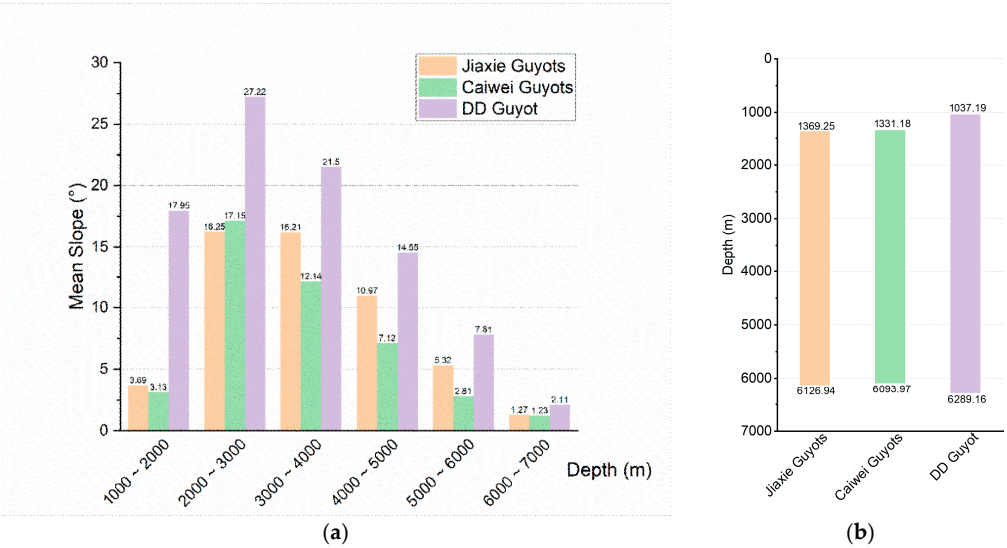


Figure 15. Morphological characteristics of (**a**) the mean slope of the distribution of guyots by depth and (**b**) guyot depth differences.

Unlike the Jiaxie Guyots and the Caiwei Guyots, the ridge is the main part of the DD Guyot, which is associated with volcanic activity forms [9–12] and guyot landslides [48]. The means of guyot formation have effects on seamount morphometrics and distribution [9,11]. There are areas of high instability on seamount slopes that make them susceptible to landslides, resulting in the formation of distinct ridges on guyots. Local crests characterize the stability of guyot slopes [33]. The exact cause needs to be analyzed in conjunction with the substrate sampling data [8,48–50].

Guyots have similar geomorphological characteristics [1,9,35]. Summit platforms contain carbonate rocks and biological remains [24]. Slope also affects the distribution of

seabed resources. For these studies, backscatter intensity and visualization data will play an important role.

5.4. Scoping of Seamounts

A comparison of guyot sections reveals that the gentle and very gentle slopes of the guyots are larger in size and that these two sections are not clearly bound by the seafloor plains. This suggests that the gradual decrease in slope from the summit towards the deep sea creates a piedmont area, which also makes the boundaries of seamounts difficult to define. In this paper, an attempt was made to delineate seamounts and submarine plains by a 2° boundary. Multiple thresholds exist for the delineation of seamount boundaries, and there are no general criteria and methods. For example, Zhang et al. [51] identified isolated seamounts in the South China Sea using 5° as the dividing line.

Some scholars have also proposed deep learning-based or dynamic planning-based methods for seabed geographic entity boundary delineation [52–55], which do not require explicit depth thresholds. How to determine the boundaries of seamounts remains a subject for study.

6. Conclusions

In this study, the geomorphologic classification of the Jiaxie Guyots, the Caiwei Guyots, and the DD Guyot was carried out, and maps of the fine-scale geomorphology types of the guyots were drawn that contain nine geomorphology types and ridgelines. To improve the accuracy, flexibility, and versatility of geomorphologic classification, a stepwise fine-scale geomorphologic identification method was proposed. Firstly, the seafloor plains, which are the part outside the mountain, were recognized, and it was ensured that those would not be confused with the mountain slopes. Secondly, the summit platforms were identified based on slope thresholds and elevation sequences. Finally, the remaining part of the mountain was divided sequentially according to slope class. Seamounts are not smooth formations with a constant change in slope, but develop a large number of local crests, local depressions, gullies on the slopes, and ridges. In this study, they were analyzed using the BPI factor, and the BPI identification results were filtered by combining two topographic factors, elevation and slope. Local crests were extracted in areas with stdBPI > 100, and local depressions and gullies on the slopes were extracted in areas with stdBPI < −100, thus overcoming, to a certain extent, the problem of the poor applicability of the BPI in fine geomorphology classification. Ridgelines were also mapped. After comparative analysis and verification, the results showed that the method can effectively realize the fine geomorphologic classification of guyots and is applicable to guyots of similar tectonics with good generality.

The determination of thresholds for some of the categorization indicators often relies on experience. For example, when selecting the radius for BPI calculation, academics have not yet established a universal determination standard based on mathematical derivation. This requires combining model principles and specific application scenarios to gradually explore reasonable threshold selection methods through experimental validation and data analysis. Artificial Intelligence (AI) models may show good results in seamount geomorphologic classification, which is worthy of in-depth study.

Author Contributions: Conceptualization, H.W., Y.S. (Yongfu Sun) and S.W.; methodology, H.W.; software, H.W.; validation, H.W., Y.S. (Yongfu Sun) and S.W.; formal analysis, H.W.; investigation, H.W., Y.S. (Yongfu Sun), W.G., W.X. and X.Y.; resources, H.W., W.G., W.X., X.Y., S.R. and Y.S. (Yihui Shao); data curation, H.W., W.G., W.X., X.Y., S.R. and Y.S. (Yihui Shao); writing—original draft preparation, H.W.; writing—review and editing, H.W., Y.S. (Yongfu Sun), S.W. and Z.L.; visualization, H.W.; supervision, Y.S. (Yongfu Sun), S.W., W.G. and Z.L.; and project administration, Y.S. (Yongfu

Sun) and W.G.; funding acquisition, S.W. and W.G. All authors have read and agreed to the published version of the manuscript.

Funding: This work was supported by the National Key Research and Development Program of China (2023YFC2812905); and the project ZR2022MD036 supported by Shandong Provincial Natural Science Foundation.

Data Availability Statement: The data presented in this study are available on request from the corresponding author due to laboratory confidentiality regulations.

Conflicts of Interest: The authors declare that the research was conducted in the absence of any commercial or financial relationships that could be construed as potential conflicts of interest.

Appendix A

The 3D maps of geomorphologic types for the Jiaxie Guyots, the Caiwei Guyots, and the DD Guyot are shown in Figures A1–A3.

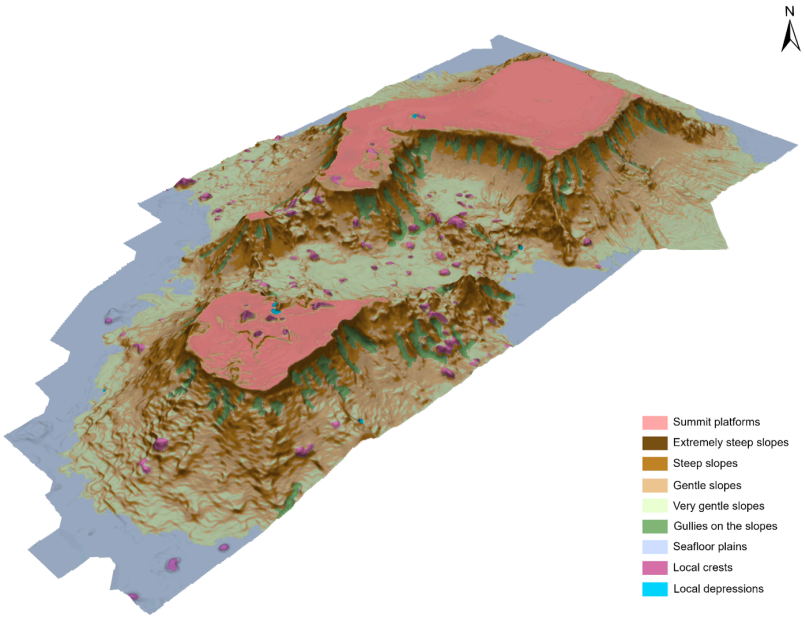


Figure A1. The 3D map of geomorphologic types for the Jiaxie Guyots.

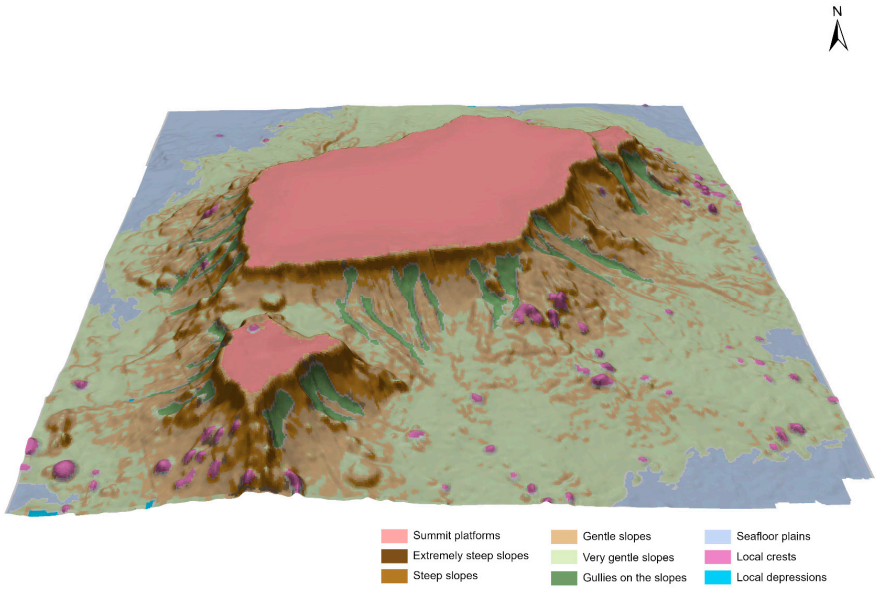


Figure A2. The 3D map of geomorphologic types for the Caiwei Guyots.

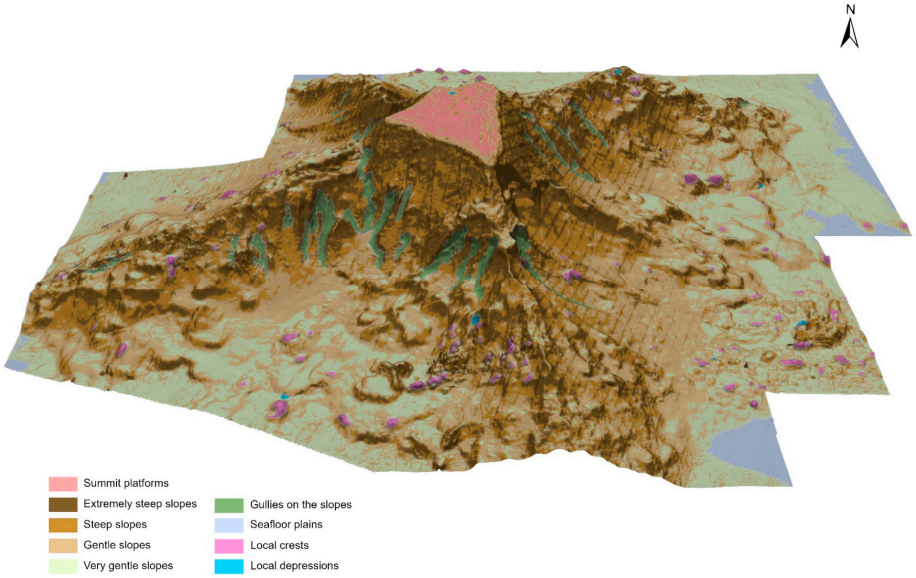


Figure A3. The 3D map of geomorphologic types for the DD Guyot.

References

1. Kim, S.-S.; Wessel, P. New Global Seamount Census from Altimetry-Derived Gravity Data. *Geophys. J. Int.* **2011**, *186*, 615–631. [CrossRef]
2. Yesson, C.; Clark, M.R.; Taylor, M.L.; Rogers, A.D. The Global Distribution of Seamounts Based on 30 Arc Seconds Bathymetry Data. *Deep Sea Res. Part Oceanogr. Res. Pap.* **2011**, *58*, 442–453. [CrossRef]
3. Hess, H.H. Drowned Ancient Islands of the Pacific Basin. *Eos Trans. Am. Geophys. Union* **1946**, *27*, 875. [CrossRef]
4. Staudigel, H.; Clague, D.A. The Geological History of Deep-Sea Volcanoes Biosphere, Hydrosphere, and Lithosphere Interactions. *Oceanography* **2010**, *23*, 58–71. [CrossRef]
5. Harris, P.T.; Macmillan-Lawler, M.; Rupp, J.; Baker, E.K. Geomorphology of the Oceans. *Mar. Geol.* **2014**, *352*, 4–24. [CrossRef]
6. Batiza, R. Abundances, Distribution and Sizes of Volcanoes in the Pacific Ocean and Implications for the Origin of Non-Hotspot Volcanoes. *Earth Planet. Sci. Lett.* **1982**, *60*, 195–206. [CrossRef]
7. Ma, J.; Song, J.; Li, X.; Yuan, H.; Li, N.; Duan, L.; Wang, Q. Environmental Characteristics in Three Seamount Areas of the Tropical Western Pacific Ocean: Focusing on Nutrients. *Mar. Pollut. Bull.* **2019**, *143*, 163–174. [CrossRef]
8. Wang, X.; Li, H.; Cheng, Y.; Yao, P.; Chu, F.; Ma, W.; Wang, H.; Lv, S.; Li, X.; Li, Z.; et al. Submarine Morphological Description of the Ancient Archipelagic Aprons in the Marcus–Wake Seamount Group, Northwestern Pacific Ocean. *J. Mar. Sci. Eng.* **2024**, *12*, 670. [CrossRef]
9. Gevorgian, J.; Sandwell, D.T.; Yu, Y.; Kim, S.-S.; Wessel, P. Global Distribution and Morphology of Small Seamounts. *Earth Space Sci.* **2023**, *10*, e2022EA002331. [CrossRef]
10. Lee, T.-G.; Lee, K.; Hein, J.R.; Moon, J.-W. Geophysical Investigation of Seamounts near the Ogasawara Fracture Zone, Western Pacific. *Earth Planets Space* **2009**, *61*, 319–331. [CrossRef]
11. Wei, X.; Zhang, Y.; Shi, X.-F.; Castillo, P.R.; Xu, Y.-G.; Yan, Q.-S.; Liu, J.-H. Co-Occurrence of HIMU and EM1 Components in a Single Magellan Seamount: Implications for the Formation of West Pacific Seamount Province. *J. Petrol.* **2022**, *63*, egac022. [CrossRef]
12. Wei, X.; Zhang, G.-L.; Zhang, J.; Shi, X.-F.; Castillo, P.R.; Zhang, Y.; Zhang, W.-F.; Xu, Y.-G.; Li, H.-Y.; Zhang, H. Overlapping Hotspot Tracks and Melts from Diffuse Plume Materials in the Upper Mantle Generated Intraplate Seamount Groups in the West Pacific. *Earth Planet. Sci. Lett.* **2024**, *643*, 118901. [CrossRef]
13. Rollinson, H.R.; Rollinson, H.; Pease, V. *Using Geochemical Data: To Understand Geological Processes*; Cambridge University Press: Cambridge, UK, 2021; ISBN 1-108-74584-9.
14. Staudigel, H.; Koppers, A.A.P. Chapter 22—Seamounts and Island Building. In *The Encyclopedia of Volcanoes*, 2nd ed.; Sigurdsson, H., Ed.; Academic Press: Amsterdam, The Netherlands, 2015; pp. 405–421, ISBN 978-0-12-385938-9.
15. Du, D.; Yan, S.; Yang, G.; Shi, F.; Zhu, Z.; Song, Q.; Yang, F.; Cui, Y.; Shi, X. Depositional Patterns Constrained by Slope Topography Changes on Seamounts. *Sci. Rep.* **2020**, *10*, 20534. [CrossRef] [PubMed]
16. Sheth, H.C.; Ray, J.S.; Bhutani, R.; Kumar, A.; Smitha, R.S. Volcanology and Eruptive Styles of Barren Island: An Active Mafic Stratovolcano in the Andaman Sea, NE Indian Ocean. *Bull. Volcanol.* **2009**, *71*, 1021–1039. [CrossRef]

17. Aswini, K.K.; KameshRaju, K.A.; Bijesh, C.M.; Yatheesh, V.; Zeba, N.F.K.; Dewangan, P. Morphotectonic Characteristics of the Andaman Volcanic Arc and Its Adjoining Regions, Andaman Sea. *Geo-Mar. Lett.* **2024**, *44*, 13. [CrossRef]
18. Yin, S.; Pope, E.L.; Lin, L.; Ding, W.; Gao, J.; Wu, Z.; Yang, C.; Chen, J.; Li, J. Re-Channelization of Turbidity Currents in South China Sea Abyssal Plain Due to Seamounts and Ridges. *Mar. Geol.* **2021**, *440*, 106601. [CrossRef]
19. Chen, Q.; Shen, J.; Ku, M.; Wang, L. Numerical Investigation of Submarine Spreading Landslide Failures. *Geotech. Geol. Eng.* **2024**, *43*, 42. [CrossRef]
20. Antunes, A.; Ngugi, D.K.; Stingl, U. Microbiology of the Red Sea (and Other) Deep-Sea Anoxic Brine Lakes. *Environ. Microbiol. Rep.* **2011**, *3*, 416–433. [CrossRef]
21. Zhao, B.; Yang, Y.; Zhang, X.; He, G.; Lü, W.; Liu, Y.; Wei, Z.; Deng, Y.; Huang, N. Sedimentary Characteristics Based on Sub-Bottom Profiling and the Implications for Mineralization of Cobalt-Rich Ferromanganese Crusts at Weijia Guyot, Western Pacific Ocean. *Deep Sea Res. Part Oceanogr. Res. Pap.* **2020**, *158*, 103223. [CrossRef]
22. Yang, Z.; Qian, Q.; Chen, M.; Zhang, R.; Yang, W.; Zheng, M.; Qiu, Y. Enhanced but Highly Variable Bioturbation around Seamounts in the Northwest Pacific. *Deep Sea Res. Part Oceanogr. Res. Pap.* **2020**, *156*, 103190. [CrossRef]
23. Sun, Q.; Song, J.; Li, X.; Yuan, H.; Ma, J.; Wang, Q. Bacterial Vertical and Horizontal Variability around a Deep Seamount in the Tropical Western Pacific Ocean. *Mar. Pollut. Bull.* **2020**, *158*, 111419. [CrossRef] [PubMed]
24. Iryu, Y.; Hino, H.; Takayanagi, H.; Sato, T.; Okamoto, N.; Suzuki, A.; Fujimaki, Y.; Usui, A. Topography, Sedimentology, and Biochronology of Carbonate Deposits on Seamounts in the JA Area, Northwestern Pacific Ocean. *Isl. Arc* **2023**, *32*, e12501. [CrossRef]
25. Sterk, R.; Stein, J.K. Seabed Mineral Resources: A Review of Current Mineral Resources and Future Developments. *Deep Sea Min. Summit Aberd. Scotl.* **2015**, *126*, 9–10.
26. Amon, D.J.; Gollner, S.; Morato, T.; Smith, C.R.; Chen, C.; Christiansen, S.; Currie, B.; Drazen, J.C.; Fukushima, T.; Gianni, M.; et al. Assessment of Scientific Gaps Related to the Effective Environmental Management of Deep-Seabed Mining. *Mar. Policy* **2022**, *138*, 105006. [CrossRef]
27. Clark, M.R. Deep-Sea Seamount Fisheries: A Review of Global Status and Future Prospects. *Lat. Am. J. Aquat. Res.* **2009**, *37*, 501–512. [CrossRef]
28. Yan, R.; Shen, C.; Zhang, D.; Li, Z.; Fang, L.; Wang, C. Predicting the Distribution of Megabenthic Communities on Deep-Water Seamounts with Cobalt-Rich Crusts in the Magellan Seamount Chain in the Northwestern Pacific Ocean. *Deep Sea Res. Part Oceanogr. Res. Pap.* **2024**, *208*, 104303. [CrossRef]
29. Masetti, G.; Mayer, L.A.; Ward, L.G. A Bathymetry- and Reflectivity-Based Approach for Seafloor Segmentation. *Geosciences* **2018**, *8*, 14. [CrossRef]
30. Sowers, D.C.; Masetti, G.; Mayer, L.A.; Johnson, P.; Gardner, J.; Armstrong, A.A. Standardized Geomorphic Classification of Seafloor Within the United States Atlantic Canyons and Continental Margin. *Front. Mar. Sci.* **2020**, *7*, 9. [CrossRef]
31. Lundblad, E.R.; Wright, D.J.; Miller, J.; Larkin, E.M.; Rinehart, R.; Naar, D.F.; Donahue, B.T.; Anderson, S.M.; Battista, T. A Benthic Terrain Classification Scheme for American Samoa. *Mar. Geod.* **2006**, *29*, 89–111. [CrossRef]
32. Fan, M.; Shi, S.; Ma, Y.; Wang, H.; Zhai, J.; Zhang, X.; Ning, P. High Resolution Geomorphological Classification of Benthic Structure on the Western Pacific Seamount. *Front. Mar. Sci.* **2022**, *9*, 1007032. [CrossRef]
33. Yang, Y.; He, G.; Liu, Y.; Ma, J.; Wei, Z.; Guo, B. Automated Multi-Scale Classification of the Terrain Units of the Jiaxie Guyots and Their Mineral Resource Characteristics. *ACTA Oceanol. Sin.* **2022**, *41*, 128–138. [CrossRef]
34. Allain, V.; Kerandel, J.-A.; Andréfouët, S.; Magron, F.; Clark, M.; Kirby, D.S.; Muller-Karger, F.E. Enhanced Seamount Location Database for the Western and Central Pacific Ocean: Screening and Cross-Checking of 20 Existing Datasets. *Deep Sea Res. Part Oceanogr. Res. Pap.* **2008**, *55*, 1035–1047. [CrossRef]
35. Chinese Ocean Mineral Resources Research and Development Association Office. *Chinese Gazetteer of Undersea Features on the International Seabed (2019)*; China Ocean Press: Beijing, China, 2020; ISBN 978-7-5210-0537-0.
36. UN; Ad Hoc Working Group of the Whole to Recommend a Course of Action to the General Assembly on the Regular Process for Global Reporting and Assessment of the State of the Marine Environment, including Socioeconomic Aspects. *The Second World Ocean Assessment. Vols. 1*; UN: New York, NY, USA, 2021; ISBN 97892111304220.
37. UN; Ad Hoc Working Group of the Whole to Recommend a Course of Action to the General Assembly on the Regular Process for Global Reporting and Assessment of the State of the Marine Environment, Including Socioeconomic Aspects. *The Second World Ocean Assessment. Vols. 2*; UN: New York, NY, USA, 2021; ISBN 97892116040062.
38. *GB/T 44060—2024*; Rules for Classification and Coding of Geomorphological Types. Ministry of Natural Resources of the People's Republic of China (Surveying, Mapping, and Geoinformation): Beijing, China, 2024.
39. Tang, G. *Geographic Information System Curriculum*, 2nd ed.; Higher Education Press: Beijing, China, 2019; ISBN 978-7-04-052355-3.
40. Horn, B.K.P. Hill Shading and the Reflectance Map. *Proc. IEEE* **1981**, *69*, 14–47. [CrossRef]
41. Weiss, A. Topographic Position and Landforms Analysis (Conference Poster). In Proceedings of the Poster Presentation, ESRI International User Conference, San Diego, CA, USA, 9–13 July 2001; Volume 200.

42. Iampietro, P.; Kvitek, R. Quantitative Seafloor Habitat Classification Using GIS Terrain Analysis: Effects of Data Density, Resolution, and Scale. In Proceedings of the 22nd Annual ESRI User Conference, San Diego, CA, USA, 8–12 July 2002; pp. 8–12.
43. Dillon, C. Modelling Submerged Coastal Environments: Remote Sensing Technologies, Techniques, and Comparative Analysis. Master's Thesis, Trent University, Peterborough, ON, Canada, 2016.
44. Gutierrez, R.R.; Escusa, F.; Almeida, R.P.; Ianniruberto, M.; Gualtieri, C. Bed Morphology Characterization of an Anabranching Bifurcation-Confluence of the Solimões River, Brazil. In *River Flow 2022*; CRC Press: Boca Raton, FL, USA, 2024; pp. 358–364.
45. Niyazi, Y.; Bond, T.; Kolbusz, J.L.; Maroni, P.J.; Stewart, H.A.; Jamieson, A.J. Deep-Sea Benthic Structures and Substrate Types Influence the Distribution of Functional Groups in the Wallaby-Zenith Fracture Zone (East Indian Ocean). *Deep-Sea Res. Part-Oceanogr. Res. Pap.* **2024**, *206*, 104268. [CrossRef]
46. Wienberg, C.; Wintersteller, P.; Beuck, L.; Hebbeln, D. Coral Patch Seamount (NE Atlantic)—A Sedimentological and Megafaunal Reconnaissance Based on Video and Hydroacoustic Surveys. *Biogeosciences* **2013**, *10*, 3421–3443. [CrossRef]
47. Mena, A.; Fernández-Salas, L.M. Optimizing Bathymetric Position Index (BPI) Calculation: An Analysis of Parameters and Recommendations for the Selection of Their Optimal Values. *Appl. Comput. Geosci.* **2024**, *23*, 100168. [CrossRef]
48. Sisavath, E.; Babonneau, N.; Saint-Ange, F.; Bachèlery, P.; Jorry, S.J.; Deplus, C.; De Voogd, B.; Savoye, B. Morphology and Sedimentary Architecture of a Modern Volcaniclastic Turbidite System: The Cilaos Fan, Offshore La Réunion Island. *Mar. Geol.* **2011**, *288*, 1–17. [CrossRef]
49. Mollison, K.C.; Power, H.E.; Clarke, S.L.; Baxter, A.T.; Hubble, T.C.T. Sedimentology, Structure, and Age of the Wide Bay Canyon Submarine Landslide on the Southeast Australian Continental Slope. *Mar. Geol.* **2020**, *419*, 106063. [CrossRef]
50. Yan, K.; Chen, J.; Zhang, T. Teleseismic Indication of Magmatic and Tectonic Activities at Slow- and Ultraslow-Spreading Ridges. *J. Mar. Sci. Eng.* **2024**, *12*, 605. [CrossRef]
51. Ho, L.V.; Nguyen, D.H.; Mousavi, M.; De Roeck, G.; Bui-Tien, T.; Gandomi, A.H.; Wahab, M.A. A Hybrid Computational Intelligence Approach for Structural Damage Detection Using Marine Predator Algorithm and Feedforward Neural Networks. *Comput. Struct.* **2021**, *252*, 106568. [CrossRef]
52. Di Stefano, M.; Mayer, L.A. An Automatic Procedure for the Quantitative Characterization of Submarine Bedforms. *Geosciences* **2018**, *8*, 28. [CrossRef]
53. Cui, B.; Wu, Z.; Zhao, D.; Yang, F.; Liu, Z.; Yao, Y.; Sun, Z. A Method of Seafloor Geographic Entity Boundary Recognition Based on D-P Algorithm and Optimal Path. *Haiyang Xuebao* **2023**, *45*, 118–129.
54. Arosio, R.; Hobley, B.; Wheeler, A.J.; Sacchetti, F.; Conti, L.A.; Furey, T.; Lim, A. Fully Convolutional Neural Networks Applied to Large-Scale Marine Morphology Mapping. *Front. Mar. Sci.* **2023**, *10*, 1228867. [CrossRef]
55. Jiang, Y.; Wu, Z.; Yang, F.; Zhao, D.; Qin, X.; Wang, M.; Wang, Q. YOLO-SG: Seafloor Topography Unit Recognition and Segmentation Algorithm Based on Lightweight Upsampling Operator and Attention Mechanisms. *J. Mar. Sci. Eng.* **2025**, *13*, 583. [CrossRef]

Disclaimer/Publisher's Note: The statements, opinions and data contained in all publications are solely those of the individual author(s) and contributor(s) and not of MDPI and/or the editor(s). MDPI and/or the editor(s) disclaim responsibility for any injury to people or property resulting from any ideas, methods, instructions or products referred to in the content.